Journal of Hydraulic Research Vol. 41, No. 2 (2003), pp. 167–177

Finite volume method for simulating extreme flood events in natural channels

Simulation des évènements hydrologiques extrêmes dans les cours d'eau naturels par une méthode en volumes finis

VALERIO CALEFFI, *Graduate Engineer and PhD student, Università degli Studi di Ferrara, Dipartimento di Ingegneria Via G. Saragat, 1 – 44100 Ferrara, Italia. Fax: +39.0532.974870; E-mail: vcaleffi@ing.unife.it*

ALESSANDRO VALIANI, *Associate Professor, Università degli Studi di Ferrara, Dipartimento di Ingegneria Via G. Saragat, 1 – 44100 Ferrara, Italia. Fax: +39.0532.974870; E-mail: avaliani@ing.unife.it*

ANDREA ZANNI, *Graduate Engineer, Università degli Studi di Ferrara, Dipartimento di Ingegneria Via G. Saragat, 1 – 44100 Ferrara, Italia. Fax: +39.0532.974870; E-mail: azanni@ing.unife.it*

ABSTRACT
The need for mitigating damages produced by extreme hydrologic events has stimulated the European Community to fund several projects. The Concerted Action on Dam-break Modelling workgroup (CADAM) performed a considerable work for the development of new codes and for the adequate verification of their performance. In the context of the CADAM project, a new 2D computer code is developed, tested and applied, as described in the present paper. The algorithm is obtained through the spatial discretisation of the shallow water equations by a finite volume method, based on the Godunov approach. The HLL Riemann solver is used. A second order accuracy in space and time is achieved, respectively by MUSCL and predictor–corrector techniques. The high resolution requirement is ensured by satisfaction of TVD property. Particular attention is posed to the numerical treatment of source terms. Accuracy, stability and the reliability of the code are tested on a selected set of study cases. A grid refinement analysis is performed. Numerical results are compared with experimental data, obtained by the physical modelling of a submersion wave on a portion of the Toce river valley, Italy, performed by ENEL–HYDRO and considered as representative of a real life flood occurrence.

RÉSUMÉ
Le besoin d'atténuer des dommages produits par des événements hydrologiques extrêmes a conduit la Communauté Européenne à développer plusieurs projets. L'action concertée du Groupe de Modélisation des Ruptures de Barrages (CADAM) a effectué un travail considérable pour le développement de nouveaux codes et pour vérifier convenablement leur exécution. Dans le contexte du projet CADAM, un nouveau code de calcul 2D est développé, testé et appliqué; c'est l'objet du présent article. L'algorithme est obtenu par la discrétisation spatiale des équations en eau peu profonde, avec une méthode de volumes finis basée sur l'approche de Godunov. On utilise le solveur de Riemann HLL. On obtient une précision du second ordre en espace et en temps, respectivement, par les techniques MUSCL et prédicteur/correcteur. La condition de haute résolution est assurée en satisfaisant la propriété TVD. Une attention particulière est portée au traitement numérique des termes sources. La précision, la stabilité et la fiabilité du code sont examinées sur un ensemble choisi de cas d'étude. Une analyse de raffinement de grille est exécutée. Les résultats numériques sont comparés aux données expérimentales provenant du modèle physique d'une onde de submersion sur une partie de la vallée de fleuve de Toce en Italie, mesures effectuées par ENEL-HYDRO et considérées comme représentatives d'une inondation réelle.

Keywords: SWE; FVM; HLL approximate Riemann Solver; source terms; overland flood flow; Toce river.

1 Introduction

The comparison between experimental data and numerical results represents an important tool for the validation of numerical codes. In this context the ENEL–HYDRO (ENEL–CRIS in the past) research group realised a physical model of a portion of Toce river valley and a hypothetical flood event on this model was reproduced. In this work an algorithm for the numerical simulation of this event is developed.

The numerical modelling of flood events on actual geometry is characterised by several problems of accuracy, stability and versatility of the used algorithms. The main problems to be solved, in order to obtain an accurate solution, are strongly dependent on the discontinuities of the solution, to the wetting-drying processes and to the abrupt changes in the bottom slope. Finally, geometrical irregularities of the computational domain require an algorithm able to work with flexible 2D meshes.

The mathematical model here described consists of the 2D Shallow Water Equations (SWE), because it is demonstrated their suitability for the simulation of free surface sharp transients; for more details look at Whitham [1], Liggett [2], Chaudhry [3], Morris [4]. Besides, a detailed description of vertical dynamics is often out of the scope of practical purposes, when the scale of interest is that of the river valley. The mathematical model is

Revision received March 5, 2002. Open for discussion till August 31, 2003.

spatially discretised using the cell-centre Finite Volume Method (FVM) approach. This choice is justified by several properties that characterise this method. First of all, the development of algorithms able to work on complex geometries, using FVM, is simple if compared with other discretisation methods, such as Finite Elements Method (FEM). Besides, FVM needs less computational effort than FEM. Finally, FVM gives conservative schemes with shock-capturing properties because, otherwise other methods, it is based on the integral form of the conservation equations [5]. For these reasons the current trend about the discretisation technique in computational fluid dynamics (CFD) seems to be represented by FVM [6–8].

The developed code belongs to the family of upwind schemes. These schemes are introduced for the solution of the hyperbolic sets of equations in order to take into account the information about the direction of signal propagation, enclosed in this class of equations.

One method is based on the solution of local Riemann problem at cell interfaces. This approach was proposed by Godunov [9], so the derived schemes are called Godunov-type. In the well known work of Godunov, the exact solution of the Riemann problem was used. Today the exact solution of the Riemann problem is replaced with an approximate solution in order to reduce computational time; this type of schemes is called Flux Difference Splitting (FDS). In the last twenty years, many efforts are done by several researchers in the field of approximate Riemann solvers. The more remarkable results are obtained in aerodynamics, but are also easily applicable to the shallow water equations. In fact, a strong analogy between compressible flow and free surface shallow water flow exists (Liggett [2]). The most reliable approximate Riemann solvers are developed by Roe [10], Van Leer [11,12], Osher and Solomon [13], Harten [14,15], and extended later on to free surface hydraulics by several workers, including Glaister [16], Alcrudo *et al*. [17], Alcrudo and Garcia-Navarro [18], Nujic [19] and Valiani *et al.* [8].

The optimal compromise between accuracy and computational heaviness is judged to be achieved by a spatial second order accuracy scheme (Hirsch [5,20]). In order to avoid oscillations of the solution near discontinuities associated to second order schemes, i.e. to obtain an high-resolution scheme, several techniques are developed. The most popular ones are based on the Total Variation Diminishing (TVD) [21], the Essentially Nonoscillatory (ENO) [22,23] or the Normalised Variable Diagram (NVD) [24] concepts.

In this work the high-resolution property is obtained using the Van Leer's Monotonic Upstream Schemes for Conservation Laws (MUSCL) approach [25] associated with the slope limiter minmod [20].

2 Algorithm description

2.1 Governing equations

The 2D shallow water equations for the simulation of a flood wave can be solved using the FVM discretisation technique, even if the solution is discontinuous. This property of SWE was accurately investigated in several works; for a recent review, look at Toro [26] and Morris [4]. Theoretical bases of the SWE theory may be found in Whitham [1], Liggett [2] and Chaudhry [3]. Complex turbulence effects are not included in the equations.

The dependent flow variables in such equations are the flow depth (h) and the x and y components of the unit discharge (hu and hv), related to the corresponding vertically averaged flow velocity components (u and v). Such variables are grouped in the column vector $\mathbf{U} = [h \;\; hu \;\; hv]^T$. The shallow water equations written in conservation form become:

$$\frac{\partial \mathbf{U}}{\partial t} + \nabla \cdot \mathbf{F} = \mathbf{S} \tag{1}$$

where $\mathbf{F} = \mathbf{F}(\mathbf{U}) = [\mathbf{E}(\mathbf{U}), \mathbf{G}(\mathbf{U})]$ is the flux vector and $\mathbf{S} = \mathbf{S}_0 + \mathbf{S}_\mathrm{f}$ is the source term with:

$$\mathbf{E} = \begin{bmatrix} hu \\ hu^2 + g\dfrac{h^2}{2} \\ huv \end{bmatrix} \quad \mathbf{G} = \begin{bmatrix} hv \\ huv \\ hv^2 + g\dfrac{h^2}{2} \end{bmatrix}$$

$$\mathbf{S}_0 = \begin{bmatrix} 0 \\ ghS_{0x} \\ ghS_{0y} \end{bmatrix} \quad \mathbf{S}_f = \begin{bmatrix} 0 \\ -ghS_{fx} \\ -ghS_{fy} \end{bmatrix} \tag{2}$$

The bottom slope in x and y directions is indicated with S_{0x} and S_{0y}. The friction slope in the same directions (S_{fx} and S_{fy}) can be estimated using empirical formulae, such as the Manning equation:

$$S_{fx} = \frac{n^2 u\sqrt{u^2+v^2}}{h^{4/3}} \quad S_{fy} = \frac{n^2 v\sqrt{u^2+v^2}}{h^{4/3}} \tag{3}$$

where n is Manning's roughness coefficient; g is the acceleration due to the gravity; t is time.

2.2 Finite volume method

The finite volume method is based on writing the mathematical model equations in integral form over an elementary control volume. Each elementary volume is represented by a cell of the mesh, used for the discretisation of the simulated domain (Liggett [2], Hirsch [5], Alcrudo and Garcia-Navarro [18]). In order to simplify the development of a second order spatial accuracy algorithm, a structured grid, composed by quadrilateral cells, is adopted.

Let us consider a single cell. Its boundary is given by union of the four straight sides enclosing it, hereafter denoted dS_r ($r = 1, \ldots, 4$). The outward normal unit vector to each side is called $\mathbf{n}_r$. Equation (1) can be integrated over the cell volume ΔV as:

$$\int_{\Delta V} \frac{\partial \mathbf{U}}{\partial t}\, dV + \int_{\Delta V} \nabla \cdot \mathbf{F}\, dV = \int_{\Delta V} \mathbf{S}\, dV \tag{4}$$

Applying the Gauss theorem, and calling $\Delta\mathbf{U}$ the time increment (in the time interval Δt) of the average of $\mathbf{U}$ over each cell, one obtains:

$$\Delta\mathbf{U} = -\frac{\Delta t}{\Delta V}\sum_{r=1}^{4}(\mathbf{F}_r^* \cdot \mathbf{n}_r)\, dS_r + \frac{\Delta t}{\Delta V}\int_{\Delta V} \mathbf{S}\, dV \tag{5}$$

The integral discretisation of the flux through the whole surface boundary of the control volume is obtained by the introduction

of a sum, over the four sides of each element, of a numerical flux function $\mathbf{F}^*$. The explicit expression of $\mathbf{F}^*$ depends on the selected approximate Riemann solver.

2.3 Godunov-type scheme

The used shallow water mathematical model is a set of hyperbolic equations that typically represents propagation phenomena. In order to correctly reproduce such physical phenomena, where the flow variables may be discontinuous, upwind schemes are developed (Hirsch [20]). A family of methods that belongs to this class of schemes is the Godunov-type ones [9]. The original Godunov method is organised in three steps. The first step consists of an approximation of the spatial distribution of the dependent variables through a piecewise constant solution over each cell. The second step is the determination of the exact solution of local Riemann problem at cell interfaces. The last step consists of a spatial average of dependent variables over each cell.

In order to reduce the computation time, the exact solution of the Riemann problem is replaced with an approximated one. The information derived from the exact solution is, in any case, partially lost in the third step, so that the loss of information due to the use of an approximate solution is not significant in practice (Hirsch [20]).

2.4 Approximate Riemann solvers

Two approximate Riemann solvers are tested. The first is due to Roe [10] and represents a classical solution, used for the implementation of Godunov type schemes and suitable to solve several CFD problems. Descriptions of this technique is herein omitted for space reasons, but can be found in several works including Roe [10], Alcrudo and Garcia-Navarro [18] and Toro [26]. The second implemented approximate Riemann solver is known as the HLL acronym, by the name of the authors (Harten, Lax and van Leer) that have proposed it in 1983 (Harten *et al*. [14]).

Generally, similar numerical results can be achieved using these different Riemann solvers. Only working on dry bed problems the HLL approach highlights a better behaviour, avoiding unidimensionalisation effects on the flow field. Such a reason leads to the choice of the HLL Riemann solver for the development of the presented code. Each result hereafter presented is obtained using such a Riemann solver; an exception is done just for the results depicted in Figure 5(d).

The application of this approach to the two-dimensional scheme gives the following expression for the numerical flux:

$$\mathbf{F}^* \cdot \mathbf{n} = \frac{s_R \mathbf{F}_L \cdot \mathbf{n} - s_L \mathbf{F}_R \cdot \mathbf{n} + s_L s_R (\mathbf{U}_R - \mathbf{U}_L)}{s_R - s_L} \tag{6}$$

where $\mathbf{n}$ is the outward normal unit vector; $\mathbf{F}_R = \mathbf{F}(\mathbf{U}_R)$ and $\mathbf{F}_L = \mathbf{F}(\mathbf{U}_L)$; subscripts R and L are referred to the right and to the left side of the cell interface respectively. The s_L and s_R symbols represent the wave speeds propagation and they can be estimated through the "two expansion" approach due to Toro [27]:

$$\begin{aligned} s_L &= \min(\mathbf{q}_L \cdot \mathbf{n} - \sqrt{gh_L}, u^* - \sqrt{gh^*}) \\ s_R &= \min(\mathbf{q}_R \cdot \mathbf{n} - \sqrt{gh_R}, u^* + \sqrt{gh^*}) \end{aligned} \tag{7}$$

where $\mathbf{q} = (u, v)$ and:

$$\begin{aligned} u^* &= \tfrac{1}{2}(\mathbf{q}_L + \mathbf{q}_R) \cdot \mathbf{n} + \sqrt{gh_L} - \sqrt{gh_R} \\ \sqrt{gh^*} &= \tfrac{1}{2}\left(\sqrt{gh_L} + \sqrt{gh_R}\right) + \tfrac{1}{4}(\mathbf{q}_L + \mathbf{q}_R) \cdot \mathbf{n} \end{aligned} \tag{8}$$

If the cell on the right or on the left of the interface is dry, Eqs. (7) become respectively:

$$\begin{aligned} s_L &= \mathbf{q}_L \cdot \mathbf{n} - \sqrt{gh_L} \qquad & s_L &= \mathbf{q}_R \cdot \mathbf{n} - 2\sqrt{gh_R} \\ & \text{and} & & \\ s_R &= \mathbf{q}_L \cdot \mathbf{n} + 2\sqrt{gh_L} \qquad & s_R &= \mathbf{q}_R \cdot \mathbf{n} + \sqrt{gh_R} \end{aligned} \tag{9}$$

2.5 High order scheme

The need of accurate solutions leads to the convenient use of a second order accuracy code, both in space and time. In order to achieve this aim, the well tested MUSCL procedure [25] and a classical predictor-corrector approach [5,20] are applied to the Godunov-type scheme.

The MUSCL procedure consists of a linear extrapolation of corresponding variables at cell interfaces, that replaces the first step of the original Godunov method (Figure 1). Unfortunately, the application of the MUSCL technique without suitable adjustments leads to an oscillatory solution near discontinuities, as demonstrated by Hirsch [20]. In order to avoid these oscillations, it is necessary to limit the extrapolated solution slope. This can be obtained introducing a non-linear function, called "limiter", of the ratio between adjacent gradients. For the characterisation of this function the total variation diminishing (TVD) property is introduced. A solution that satisfies this condition is non-oscillatory, of an order of accuracy greater than one, and preserving monotonicity. Several limiters are described in literature [20]. In this work different limiters are tested, even if the corresponding results are not presented. Working on a wet bed, no significant differences of performance are observed between different limiters, whereas the "minmod" limiter shows a better ability to avoid non-physical negative depths working on a dry bed.

2.6 Source terms

Extensive literature is available to discuss the treatment of the homogeneous part of the flow motion equations. In these works theoretical examples without friction and bottom slope are presented (e.g. [5,17,18,20,28–30]).

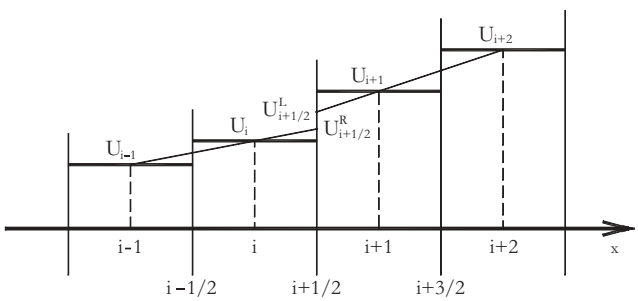

Figure 1 Sketch of the linear variable extrapolation at the cell interface.

In the solution of problems involving real geometries, a correct treatment of source terms is necessary to obtain accurate results. Published works about these problems are rarer. Only recently, relevant issues were achieved in the development of numerical techniques, that lead to a balancing of source terms and flux gradients, at least in the asymptotic case of quiescent fluid over irregular geometries (Hubbard and Garcia-Navarro [31], Garcia-Navarro and Vazquez-Cendon [32]). Unfortunately, these contributions concern numerical schemes based on the Roe's approximate Riemann solver. An extension of this approach to schemes based on different Riemann solvers (e.g. the HLL one) seems to lead to a quite complex formulation, that is worthy of further investigation but it is not immediately available for engineering purposes. The previously described lack in the source terms treatment in the HLL-based computer codes, coupled to the practical purpose to formulate a simple approach to the problem of bottom irregularities handling, have led to the development of the original technique herein presented.

2.6.1 Bottom slope source terms

The numerical treatment of the bottom slope source terms ($\mathbf{S}_0 = [0 \quad ghS_{0x} \quad ghS_{0y}]^T$ is not trivial, because the four vertices of each cell, generally, do not lie on the same plane. An explicit, four step process is adopted here (Figure 2):

(i) The first step is the determination of the planimetric position of the centroid (G) of a generic cell. In order to estimate the altimetric co-ordinate of G, an average of the four vertices elevation, weighted with the distances between each vertices and the centroid, is used.

(ii) In the second step, the single cell is shared into four triangular elements, with a common vertex coincident with G (sub-cells). Each sub-cell lies on a plane. Such a plane is considered a local approximation of the real bottom.

(iii) The third step is constituted by the determination of the equation of the plane, relative to each sub-cell, and of its slope along x and y directions.

(iv) The fourth step consists of the division of the surface integral on the cell into four surface integrals on the sub-cells.

The constancy of bottom slope for each triangular element allows the corresponding integral to be expressed as a constant times a volume. The constant depends on the bottom slope and the volume is that of the water prism over each sub-cell.

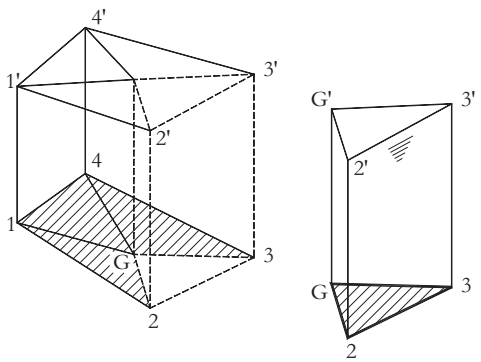

Figure 2 In order to evaluate the bottom slope source terms, each quadrangular cell is divided in four triangular sub-cells; each group of three vertices uniquely identifies a plane, that is considered to approximate the real bottom.

2.6.2 Slope friction source terms

In order to reduce the numerical instability relative to the slope friction source terms ($\mathbf{S}_\mathrm{f} = [0 \quad -ghS_{fx} \quad -ghS_{fy}]^T$, a simple semi-implicit treatment is used. Introducing an appropriate coefficient, β, to weight the variables at current time step, and a coefficient $(1-\beta)$ to weight the variables at the previous time step, one obtains (superscripts are used as time-indexes):

$$\mathbf{S}_\mathrm{f} = (1-\beta)\mathbf{S}_\mathrm{f}^{k-1} + \beta\mathbf{S}_\mathrm{f}^{k} \tag{10}$$

Introducing the jacobian matrix $\mathbf{Q}_\mathrm{f} = \partial\mathbf{S}_\mathrm{f}/\partial\mathbf{U}$, after some algebraic manipulation, the expression of the increment of $\mathbf{U}$ becomes:

$$\Delta\mathbf{U} = \left[\mathbf{I} - \Delta t\beta\mathbf{Q}_\mathrm{f}^{\mathrm{k}-1}\right]^{-1}\cdot\left[-\frac{\Delta t}{\Delta V}\sum_{r=1}^{4}(\mathbf{F}_r^{*}\cdot\mathbf{n}_r)\,dS_r + \Delta t\mathbf{S}_\mathrm{f}^{\mathrm{k}-1}\right] + \Delta t\mathbf{S}_0^{\mathrm{k}-1} \tag{11}$$

Contribution to the energy loss due to side-walls effects can be modelled introducing, at the boundary cells, appropriate corrections to these friction terms (Brufau and Garcia-Navarro [33]). In the numerical model, herein presented, such effects are neglected. This is possible because, working on real-world geometries, the typical width to depth ratio of the main flow is of the order of some tens, so that friction effects due to the bottom are much more important than friction effects due to side-walls.

3 Some test cases

In order to verify the stability of the algorithm and the reliability of the numerical results, the developed code is applied to a set of classical test cases. Most of them are suggested by CADAM. Only few examples of the used test cases are presented in this work, just for space reasons. For a detailed description of the complete set of CADAM test cases see Toro *et al.* (in Morris [4]). Other model problems, not suggested by CADAM, are used in order to verify the ability of the present code to reproduce 2D peculiarities of the flow (Fennema and Chaudhry [28], Alcrudo and Garcia-Navarro [18]).

3.1 1D transcritical steady flow with shock over a bump without friction

The aim of this test case is to study the ability of the code to correctly represent the critical transition. The shock capturing property is also verified. This example is considered as significant in order to put into evidence the correctness of the herein proposed treatment for the bottom slope source terms, that is particularly relevant in such a test case.

The spatial domain is represented by a 25×1 m rectangular cross section channel (discretised using 0.1 m length size square

cells). The bottom is frictionless and its elevation (z_b) is described by the following function:

$$z_b(x) = \begin{cases} 0 & \text{if } x < 8\,\text{m}; \\ 0.2 - 0.05(x-10)^2 & \text{if } 8 \le x \le 12\,\text{m}; \\ 0 & \text{if } x > 12\,\text{m}; \end{cases} \qquad (12)$$

The upstream flow is equal to 0.18 m^3/s and the downstream level is set equal to 0.33 m. The initial water level is 0.33 m and the initial discharge is set to 0. The analytical reference solution is obtainable through application of Bernoulli's theorem [34].

Figure 3 shows a good agreement between the water profile, given by the analytical solution, and the corresponding numerical solution. The discrepancy between analytical and numerical solution in terms of unit width discharge is intentionally emphasised by the choice of a narrow range on the vertical axis (the aim of this setting is to highlight the solution behaviour in correspondence of the bottom slope change). Really, the mean square errors of the non-dimensional solution, in terms of depth and of unit width discharge, are comparable (they are respectively 2.2×10^{-4} and 2.7×10^{-4}).

3.2 2D oblique hydraulic jump

This test case considers an oblique hydraulic jump, due to the interaction between a supercritical steady flow and a convergent vertical wall which form an angle of 8.95° with the direction of the undisturbed current. The spatial domain is represented by a 40×30 m convergent rectangular cross section channel. Such a domain is discretised using a regular 40×30 cells mesh. The bottom is flat and frictionless. The upstream boundary conditions are represented by a flow velocity equal to 8.57 m/s and a water level equal to 1 m; upstream undisturbed Froude number is 2.74.

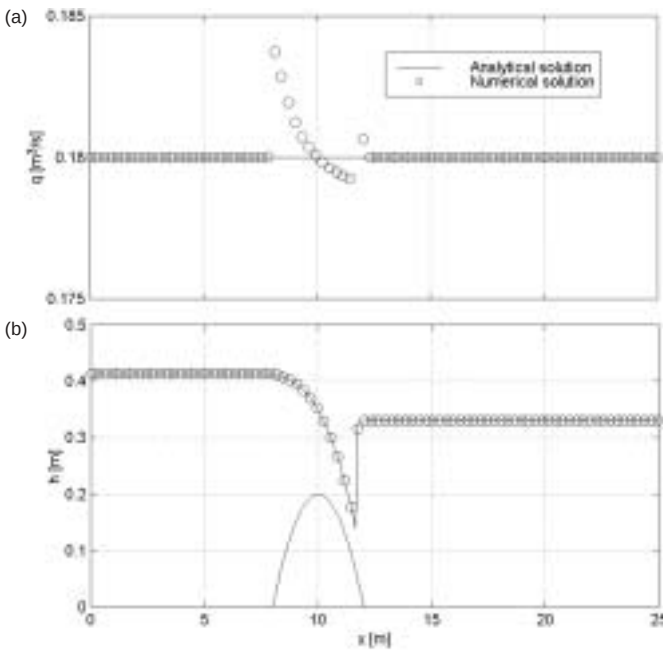

Figure 3 Comparison between analytical and numerical solution: (a) unit width discharge; (b) water level; only one point each three of the numerical solution is plotted, in order to increase the readability of the figure.

The analytical reference solution for this test case is available in literature [1,35].

Figure 4 shows the appropriate behaviour of the code. In particular, the error on the computed Mach angle is of 0.74%, while the mean square errors of the non-dimensional solution in terms of water depth and flow velocity are respectively 1.5×10^{-4} and 3.1×10^{-5}. The same estimate, referred to the Froude number, is 2.7×10^{-3}.

3.3 2D partial instantaneous dam-break over dry bed without friction

The aim of this test case is to study the ability of the code to simulate the front wave propagation over dry bed, with particular attention to the 2D aspect of the flow motion. The spatial domain is represented by a 200×200 m flat region. The bottom is frictionless. The upstream flow is equal to 0 and the downstream level is set equal to 0. The initial water level is 10 m upstream and 0 downstream. The breach is 75 m wide. The domain is discretised by 1 m side square cells. The duration of the simulation is 6 s. There is no analytical reference solution for this test case, but numerical results of various authors are available (Wang *et al*. [29], Sleigh *et al*. [36]).

Figures 5(a) and (b) show a behaviour that is in general agreement with the quoted literature; in particular, Figure 5(a) is in very good agreement with the sketches published by Sleigh *et al*. [36]. Such sketches represent numerical results obtained by a FVM scheme for adaptive, unstructured meshes.

3.4 2D partial instantaneous dam-break over wet bed without friction

The aim of this test case is to study the code ability to reproduce discontinuous solutions, with particular attention to the 2D aspect of the flow motion. The spatial domain and its discretisation is the same of the previous test case. The upstream flow is equal to 0 and the downstream level is set equal to 5 m. The initial water level is 10 m upstream and 5 m downstream. The duration of simulation is 6 s. There is no analytical reference solution for this test case, but numerical results of various authors are available (i.e. [7,18,28–30,36]) and [37] for a movable bed example). Figures 5(c) and (d) show a general agreement with existing results.

In particular, Figure 5(d) shows the good agreement of different numerical results, obtained using Roe and HLL Riemann solvers respectively; such an agreement is especially strong in terms of front wave celerity. Minor discrepancies are obtained only in the lateral portions of the wave front. Roe solver leads to a larger spreading of the submersion wave.

4 Simulation of a flood event on the Toce river valley

4.1 Physical simulation description

A further test case is based on the physical simulations performed on a 1 : 100 scale model of a reach of the Toce river valley (located

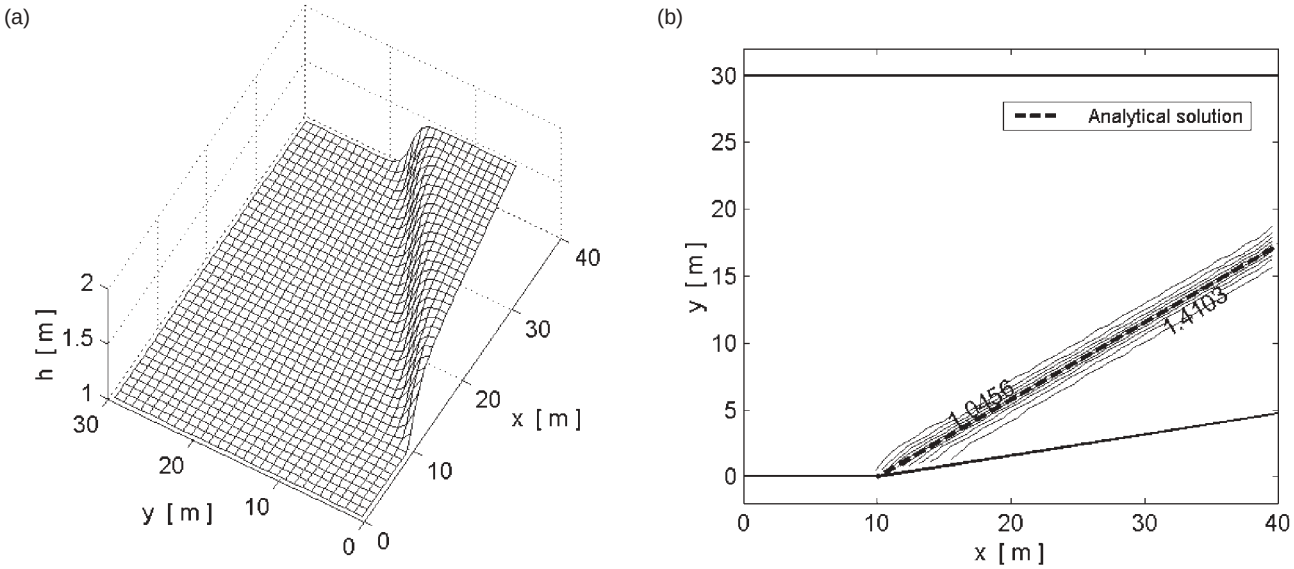

Figure 4 Interaction between a supercritical steady flow and a convergent wall: (a) water level; (b) depth contour levels. Dashed line shows the analytical location of the oblique shock.

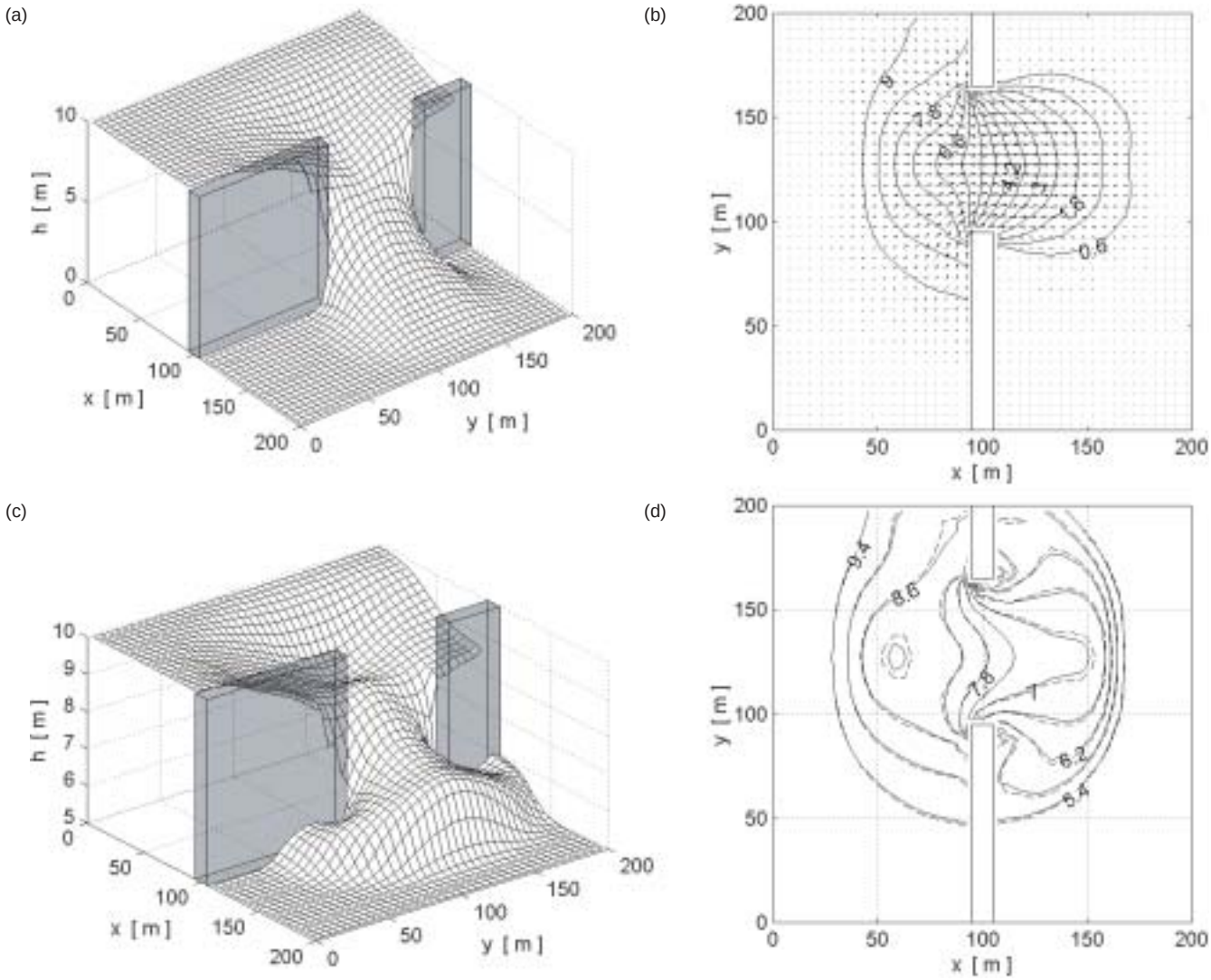

Figure 5 Dam-break test cases results: (a) water profile, dry bed case; (b) depth contour levels and unit width discharge, dry bed case; (c) water profile, wet bed case; (d) depth contour levels (dashed line: Roe Riemann solver; solid line; HLL Riemann solver), wet bed case.

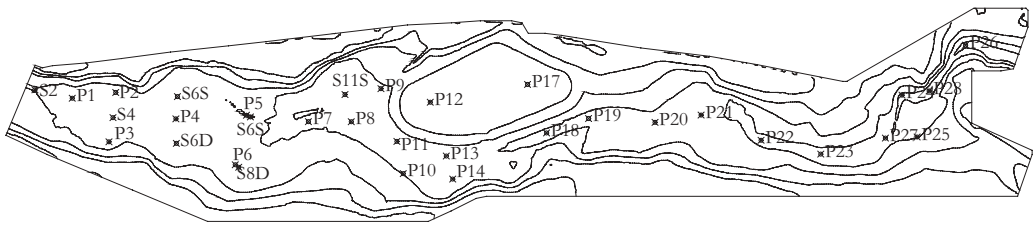

Figure 6 Bottom contour levels of the physical model and gauges position.

on the occidental Alps, Italy). Such a model is fulfilled at the ENEL-HYDRO laboratories in Milan.

The reach has several geometrical irregularities, that lead to the coexistence of subcritical and supercritical flow states (Figure 6). The model is built in concrete and its dimensions are approximately 50 × 11 m. The model reproduces the main channel and flood plains, including some buildings, two bridges, a barrage and a reservoir. A set of 33 water probes record the time evolution of water depth in different points of the physical domain. The inflow is controlled by a computer regulating a pump, with a maximum discharge of 0.5 m^3/s. The model has a free overfall at the downstream end, and it is initially dry (Testa [38]). The results of the simulations, consisting of the water depth recorded by the gauges, are given in tabular form. The duration of the simulations is 180 s.

4.2 Numerical simulation description

4.2.1 Mesh generation

The generation of the meshes is performed by utilising the commercial software SMS™ (Surface-water Modelling System) 5.06 product by BOSS® International.

The numerical description of the physical model consists of about 141,000 points of known co-ordinates that, projected on an horizontal plane, form a quadrangular grid of 5 cm size.

A mesh directly obtained by joining all the points of known co-ordinates yields a non-manageable data set. For this reason some numerical grids with less elements are developed and tested. In the following, results obtained adopting a "refined" mesh of 34,981 cells are presented. A first, coarser, mesh of 8,750 cells was previously used; the comparison between results obtained using the "coarse" mesh and the "refined" mesh allows to perform a grid refinement analysis. The coarser mesh is obtained holding one point each four (sides cells are 20 cm length), the refined mesh is obtained holding one point each two of the original data set (sides cells are 10 cm length).

As seen above, the second order accuracy in space is achieved through use of the MUSCL technique. This approach requires the use of a quadrangular structured grid. This kind of mesh is generally less adaptable to complex domains than a triangular unstructured grid. In order to reduce this limitation, the code is made to work with meshes that are obtained by joining separated structured blocks.

4.2.2 Boundary and initial conditions

Each lateral side of the simulation domain is not reached by the flow; therefore a simple wall-condition can be used.

The first attempt hypotheses that the flow at both upstream and downstream sections is in critical condition, initially proposed by the ENEL–HYDRO group, are not well verified. Numerical results, obtained from simulations using a critical or subcritical upstream boundary condition, do not fit the experimental data. So, a supercritical flow is supposed to exist upstream and, as a consequence, two conditions are imposed at the upstream section. A known discharge is imposed according with the given diagram, obtained recording the pump outflow; such a discharge is partitioned between the cells adjacent to the inflow section (first row of cells), assuming a uniformly distributed velocity over the upstream cross section itself. A water level is also imposed, according with the value recorded by S2 gauge. The flow obtained by such a method is effectively supercritical. It is necessary to highlight that a one-dimensionalisation procedure is performed at the inflow boundary, but more refined hypotheses are not supported by the presently available experimental data. Without any specific information regarding the unit discharge distribution at the inflow boundary and the water level variability at the same boundary, the herein made choice is the simplest one.

Regarding the downstream boundary, an adaptable condition is assumed: such a condition is set as critical if the water depth is higher than critical depth, and it is set as supercritical if the water depth is lower than critical depth: that is, no conditions at all are posed, if the flow is supercritical.

The dry bed hypothesis is assumed as initial condition.

4.3 Results

In the following pages three figures are shown (any result, herein presented, is directly referred to the model scale). Figure 7 illustrates the vector plot of the unit width discharge and a 3D representation of the water profile in the upstream portion of the model (Figure 7, subplot a and b) and in the reservoir region (Figure 7, subplot c and d), respectively at t = 17 s and at the end of the simulation (t = 180 s). The flow features highlighted in such a sketch are just an example of how powerful might be such a representation from the point of view of civil protection management, risk control planning, public administrations evacuation planning, land users and environmental engineering design.

Figure 8 consists of the comparison between calculated water level and recorded water level at some gauges. Results obtained using both the meshes (34,981 vs. 8,750 cells) are reported, in order to describe the main effects of mesh refinement. A general good agreement between the two series of numerical water level and experimental data is shown (Figure 8, gauges P2, P8,

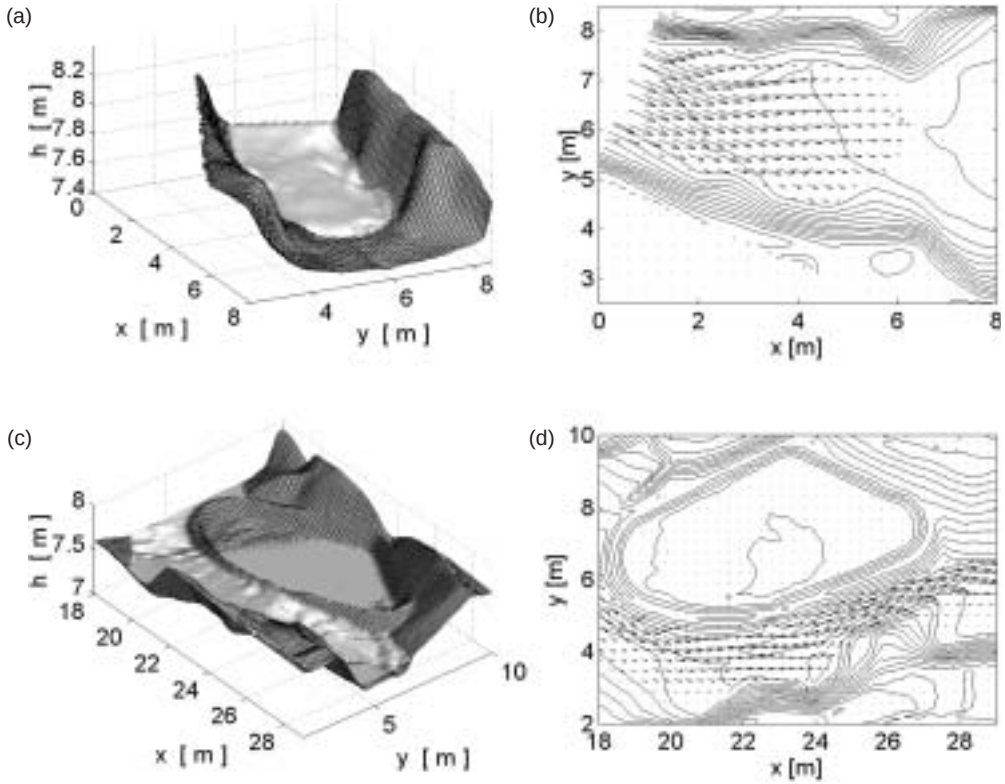

Figure 7 Water profile 3D representation and unit width discharge vectorplot: (a) and (b) upstream portion of the model, t = 17 s; (c) and (d) reservoir region, t = 180 s.

P9, P18, P19, P25 and S6S). Only the plot regarding the gauge P12 (located into the reservoir) shows a substantial differences between the results obtained adopting different grids. The former results (coarser mesh) highlight two subsequent inflow in the reservoir, instead of the only one shown in the latter results (finer mesh); moreover, the final water level of the stored liquid in the former case is higher then the latter. This behaviour is probably due to the approximations done in the numerical modelling of the embankment and, in particular, to an under-estimated height of such a structure leading to an over-estimated simulated inflow discharge in the reservoir. The local elevation of the top of the embankment is set equal to the elevation of the local highest cell vertex. Such a vertex may actually corresponds to a physical point on the crest or may corresponds to a physical point on the side of the embankment, because a grid adaptation to the bottom gradients is not performed here. If such a point belongs to the top of the embankment, the height of such a structure is correctly reproduced, if such a vertex belongs to the bank side, the height is under-estimated. The greater is the distance between the highest cell vertex and the crest of the embankment, the greater is the under-estimate of the structure height. Obviously, the greater is the characteristic linear size of the cell mesh, the greater is, generally, such a distance.

In subsequent plots, the water free surface elevation is reported vs. time. The assumption of a dry bed initial condition leads to recorded physical water depths and to corresponding simulated values that are initially zero. For this reason, at the beginning of the simulation, the bottom elevation of any gauge location appears as water level elevation. A discrepancy exists, between experimental bottom elevation and computed bottom elevation, because the planimetric positions of the two gauges is not the same. Bottom elevations and corresponding water levels are computed in the cell centroid, whilst gauges are not installed in such centroids. The nearest centroid to any gauge position is chosen as representative of the position itself. Therefore, the initial discrepancy is due to some shift in the position of the gauges. Results may be trivially improved interpolating gauges positions between the four nearest centroids. Such an operation is intentionally omitted, as a methodological choice, in order to present "clean" results, not affected by a spurious *a posteriori* interpolation.

In Figure 9, the state of the flow (subcritical or supercritical) along the valley is depicted, at 180 s from the start of the simulation. As specified before, it is shown here that the flow is characterised by several transitions through the critical state. Observing Figure 9, at x = 6.0 m the valley shows a narrowing, which leads to an upstream jump formation. Similar flow configuration can be noted, in the same figure, at x = 26 m. A numerical code able to correctly represent such transitions through the critical state (from supercritical to subcritical states and vice versa), like the developed one, is necessary in order to obtain reliable results. The presented results do not depend significantly on grid size (this is proven by grid refinement calculations) or from non-physical parameters, such as β. The substantial independence of physical parameters from non-physical parameters is accurately investigated, in order to support the validity of the present computer code. In practice, we can say that none tuning parameter must be used, in order to obtain physically based, meaningful results. Minor discrepancies between numerical results and

physical ones must be attributed to the intrinsic limits of validity of shallow water scheme. So, particular attention should be devoted to that areas, in the flow field, where streamline curvature is important (non-hydrostatic pressure distribution), and/or important recirculation phenomena take place (turbulence modelling).

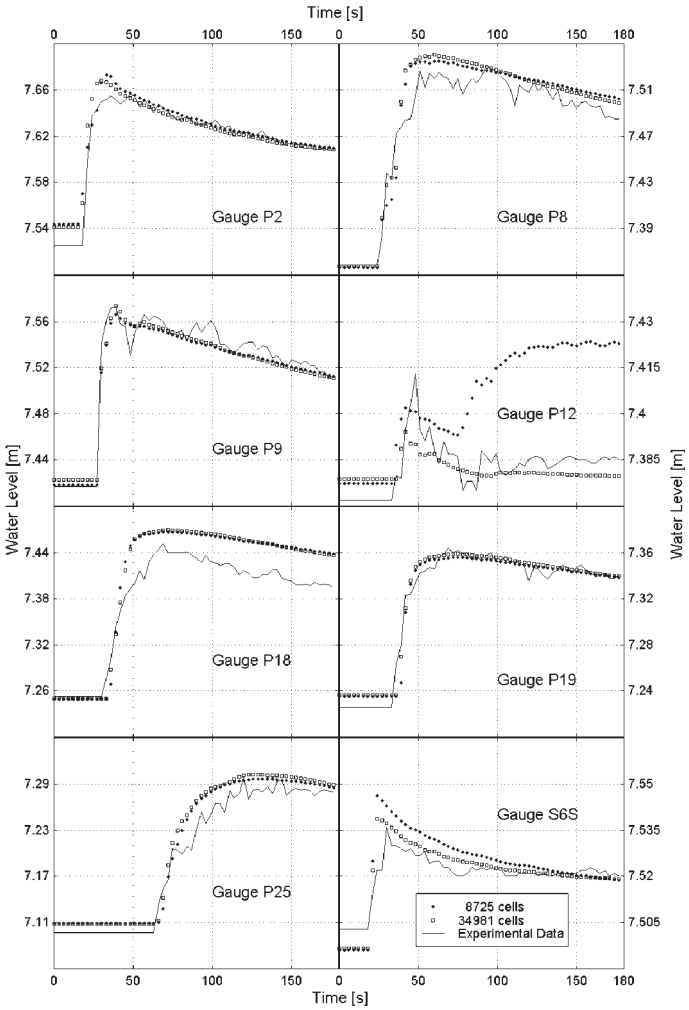

Figure 8 Comparison between measured versus simulated water levels obtained using two different meshes (34,981 vs. 8,750 cells).

Conclusions

In this work a comparison between physical model data and numerical results, obtained with a new explicit high resolution TVD algorithm, is presented.

The experimental data used in this work are derived from a simulation on a physical model realised by ENEL–HYDRO (ENEL–CRIS in the past) in its laboratories in Milan, Italy. This model reproduce a portion of Toce river valley.

The used algorithm is based on the 2D SWE. The spatial discretisation is done by a cell-centred FVM. The code belongs to the family of the Godunov-type scheme and is second order accurate both in space and time. The selected approximate Riemann solver is based on the work of Harten, Lax and Van Leer (HLL). The source terms relative to the bottom friction are discretised in a semi-implicit way, while the source terms relative to the bottom slope are treated using an original technique, essentially based on a simple geometric representation of the water volume between the free surface and the bottom surface.

In order to verify stability, accuracy and reliability of the code the algorithm is applied to a large set of test cases. Such an analysis highlights the shock-capturing property and the ability to correctly represent the transition through the critical state of the method. The code results suitable both for steady and unsteady flows, moreover it correctly reproduces the drying-wetting-drying process. 2D features of the simulated flows are adequately reconstructed.

A grid refinement analysis is performed; the code behaviour is resulted weakly dependent on the mesh size, except in correspondence of strong bottom elevation gradients near linear singularities.

The comparison between numerical results of the flood event simulation on the valley of Toce river and available experimental data allows to advance the following considerations. Generally, a good agreement between recorded water level and simulated water level is shown. The vector plots of flow velocities and the 3D representation of the portion of flooded domain show a realistic behaviour, and may represent an immediate tool in order to lay out emergency planning, risk management and interventions design.

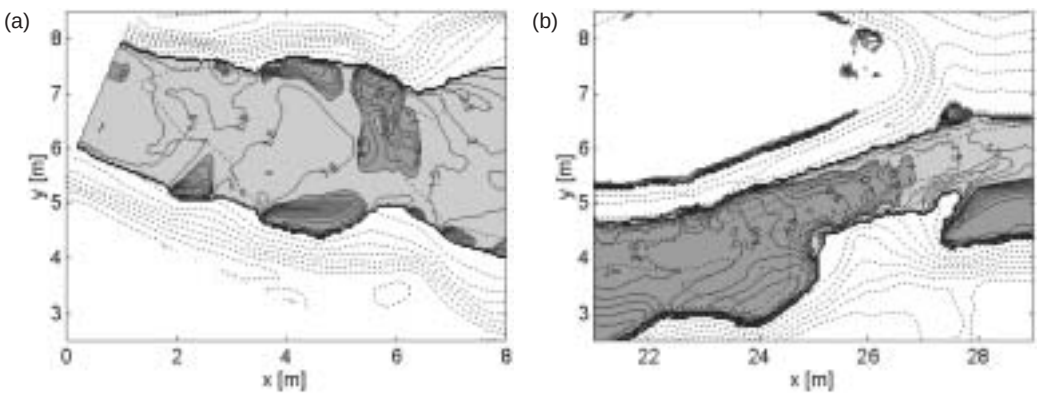

Figure 9 Representation of the state of the flow (subcritical or supercritical) in two meaningful portion of the physical domain (dark grey: subcritical state; light grey: supercritical state).

The validation of the developed code have shown some problems for which further investigation is hoped for. On working on dry, rough bottom, the appearance of negative depths requires the development of some expedient, according to the continuity law, in order to avoid this unphysical effect. Mobile bed extension and morphological computations will be further developments of the model.

Acknowledgements

The authors express their sincere thanks to the research group of ENEL–HYDRO, Italy, for experimental data and all information necessary to make this work possible. The same corporation has partially funded this investigation (CFR contract no. R/ENEL/VAL/1/00).

Notation

β = coefficient of implicity
ΔV = control volume
dS = cell side
$\mathbf{E}$ = x-component of flux vector
$\mathbf{F}$ = flux vector = [$\mathbf{E}$, $\mathbf{G}$]
$\mathbf{F}^*$ = numerical flux function
$\mathbf{F}_\mathrm{L}$ = $\mathbf{F}$ on the left cell interface
$\mathbf{F}_\mathrm{R}$ = $\mathbf{F}$ on the right cell interface
g = gravitational constant
$\mathbf{G}$ = y-component of flux vector
h = flow depth
h_L = water depth on the left cell interface
h_R = water depth on the right cell interface
$\mathbf{I}$ = identity matrix
n = Manning's roughness coefficient
$\mathbf{n}$ = outward normal unit vector
$\mathbf{Q}$ = vector of averaged velocity = [u, v]
$\mathbf{Q}_\mathrm{f}$ = jacobian matrix of $\mathbf{S}_\mathrm{f}$
$\mathbf{q}_\mathrm{L}$ = $\mathbf{q}$ on the left cell interface
$\mathbf{q}_\mathrm{R}$ = $\mathbf{q}$ on the right cell interface
$\mathbf{S}$ = vector of source terms
$\mathbf{S}_0$ = vector of bottom slope source terms
S_{0x} = x-component of bottom slope
S_{0y} = y-component of bottom slope
$\mathbf{S}_\mathrm{f}$ = vector of friction slope source terms
S_{fx} = x-component of friction slope
S_{fy} = y-component of friction slope
s_L = wave speed on the left cell interface
s_R = wave speed on the right cell interface
t = time
u = averaged flow velocity along x direction
$\mathbf{U}$ = vector of conservative variables
$\mathbf{U}_\mathrm{L}$ = $\mathbf{U}$ on the left cell interface
$\mathbf{U}_\mathrm{R}$ = $\mathbf{U}$ on the right cell interface
v = averaged flow velocity along y direction
x = x Cartesian co-ordinate
y = y Cartesian co-ordinate
z_b = bottom elevation

References

1. WHITHAM, G.B. (1974). "Linear and Nonlinear Waves", J. Wiley & Sons.
2. LIGGETT, J.A. (1994). "Fluid Mechanics", McGraw-Hill, Inc.
3. CHAUDHRY, M.H. (1993). "Open-Channel Flow", Prentice-Hall, Inc.
4. MORRIS, M. (ed.) (1998). 2nd CADAM Meeting Proceedings, HR Wallingford, 2/3 March.
5. HIRSCH, C. (1988). "Numerical Computation of Internal and External Flows", J. Wiley & Sons, Chicester, Vol. I.
6. BELLOS, C., SOULIS, J. and SAKKAS, J. (1991). "Computation of Two Dimensional Dam Break Induced Flow", *Adv. in Water Resour.*, 14(1), 31–41.
7. ZHAO, D.H., SHEN, H.W., TABIOS, G.Q., LAI, J.S. and TAN, W.Y. (1994). "Finite-volume Two-dimensional Unsteady-flow Model for River Basins", *JHE*, 120(7), 863–883.
8. VALIANI, A., CALEFFI, V. and ZANNI, A. (2002). "Case Study: Malpasset Dam-Break Simulation Using a 2D Finite Volume Method", *JHE*, 128(5), 460–472.
9. GODUNOV, S. (1959). "A Difference Scheme for Numerical Computation of Discontinuous Solution of Hydrodynamic Equations", *Math. Sbornik*, 43, 271–306.
10. ROE, P.L. (1981). "Approximate Riemann Solvers, Parameter Vectors, and Difference Schemes", *J. Comp. Physics*, 43, 357–372.
11. VAN LEER, B. (1973). "Towards the Ultimate Conservative Difference Scheme, I. The Quest of Monotonicity", *Lecture notes in Phys.*, 18, 163–168.
12. VAN LEER, B. (1977). "Towards the Ultimate Conservative Difference Scheme, III", *J. Comp. Physics*, 23, 263–275.
13. OSHER, S. and SOLOMON, F. (1982). "Upwind Difference Schemes for Hyperbolic Conservation Laws", *Math. Comp.*, 38(158), 339–374.
14. HARTEN, A., LAX, P.D. and VAN LEER, B. (1983). "On Upstream Differencing and Godunov-type Schemes for Hyperbolic Conservation Laws", *SIAM Rev.*, 25(1), 35–61.
15. HARTEN, A. (1983). "High Resolution Schemes for Hyperbolic Conservation Laws", *J. Comp. Physics*, 49, 357–393.
16. GLAISTER, P. (1988). "Approximate Riemann Solutions of the Shallow Water Equations", *JHR*, 26(3), 293–306.
17. ALCRUDO, F., GARCIA-NAVARRO, P. and SAVIRON, J.M. (1992). "Flux Difference Splitting for 1D Open Channel Flow Equations", *Int. J. Num. Methods in Fluids*, 14, 1009–1018.
18. ALCRUDO, F. and GARCIA-NAVARRO, P. (1993). "A High-resolution Godunov-type Scheme in Finite Volumes for the 2D Shallow-water Equations", *Int. J. Num. Methods in Fluids*, 16, 489–505.
19. NUJIC, M. (1995). "Efficient Implementation of Non-oscillatory Schemes for the Computation of Free Surface Flow", *JHR*, 33(1), 101–111.

20. HIRSCH, C. (1988). "Numerical Computation of Internal and External Flows", J. Wiley & Sons, Chicester, Vol. II.
21. LOUAKED, M. and HANICH, L. (1988). "TVD Scheme for the Shallow Water Equations", *JHR*, 36, 363–378.
22. TSENG, M.H. (1999). "Explicit Finite Volume Non-oscillatory Schemes for 2D Transient Free-surface Flows", *Int. J. Num. Methods in Fluids*, 30, 831–843.
23. YANG, J.Y. and HSU, C.A. (1996). "Computations of Free Surface Flows, Part 3: Steady Supercritical Flow Using a Generalized Lagrangian Method", *JHR*, 34(1), 77–98.
24. JASAK, H., WELLER, H.G. and GOSMAN, A. D. (1999). "High Resolution NVD Differencing Scheme for Arbitrarily Unstructured Meshes", *Int. J. Num. Methods in Fluids*, 31, 431–449.
25. OSHER, S. (1985). "Convergence of Generalized MUSCL Schemes", *SIAM J. Num. Analysis*, 22(5), 947–961.
26. TORO, E. (1999). "Riemann Solvers and Numerical Methods for Fluid Dynamics", Springer Verlag, Berlin.
27. TORO, E. (1992). " Riemann Problems and the WAF Method for Solving the Two-dimensional Shallow Water Equations", *Philosophical Trans. Royal Soc.* London, U.K., A338, 43–68.
28. FENNEMA, R.J. and CHAUDHRY, M.H. (1990). "Explicit Methods for 2D Transient Free-Surface Flows", *JHE*, 116(8), 1013–1034.
29. WANG, J.S., NI, H.G. and HE, Y.S. (2000). "Finite-difference TVD Scheme for Computation of Dam-break Problems", *JHE*, 126(4), 253–262.
30. AMBROSI, D. (1995). "Approximation of Shallow Water Equations by Roe's Riemann Solver", *Int. J. Num. Methods in Fluids*, 20, 157–168.
31. HUBBARD, M.F. and GARCIA-NAVARRO P. (2000). "Flux Difference Splitting and the Balancing of Source Terms and Flux Gradients", *J. Compu. Physics*, 165(1), 89–125.
32. GARCIA-NAVARRO, P. and VAZQUEZ-CENDON, M.E. (2000). "On Numerical Treatment of the Source Terms in the Shallow Water Equations", *Computers & Fluids*, 29(8), 951–979.
33. BRUFAU, P. and GARCIA-NAVARRO, P. (2000). "Two-dimensional Dam Break Flow Simulation", *Int. J. Num. Methods in Fluids*, 33(1), 35–58.
34. BERNOULLI, D. (1738). "Hydrodinamica sive de viribus et motibus fluidorum commentarii", Strasbourg.
35. IPPEN, A.T. and KNAPP, R.T. (1939). "Proc. fifth international congress of applied mechanics", J. Wiley & Sons.
36. SLEIGH, P.A., GASKELL, P.H., BERZINS, M. and WRIGHT, N.G. (1998). "An Unstructured Finite-volume Algorithm for Predicting Flow in Rivers and Estuaries", *Computers & Fluids*, 27(4), 479–508.
37. VALIANI, A. (1992). "Rapid Transients in Free-surface Flows With Movable Bed: A 2D Numerical Solution", HYDROCOMP '92, International Conference on Interaction of Computational Methods and Measurements in Hydraulics and Hydrology, Budapest, Hungary, 139–146.
38. TESTA, G. (ed.) (1999). 3rd CADAM Meeting Proceedings, Milan, Italy, 6/7 May.